ELSEVIER

Journal of Molecular Catalysis A: Chemical 155 (2000) 31–41

JOURNAL OF MOLECULAR CATALYSIS A: CHEMICAL

www.elsevier.com/locate/molcata

In situ vibrational spectroscopic investigation of surface redox process of vanadyl pyrophosphate

Gaku Koyano *, Takaya Saito, Makoto Misono

Department of Applied Chemistry, Graduate School of Engineering, The University of Tokyo, 7-3-1 Hongo, Bunkyo-ku, Tokyo 113-8656, Japan

Received 28 December 1998; accepted 19 February 1999

Abstract

Redox properties of the surface of vanadyl pyrophosphate ($(VO)_2P_2O_7$) have been investigated mainly by means of in situ Raman spectroscopy as well as IR measurement of low temperature adsorption of CO. The results of in situ Raman spectroscopy were consistent with our previous conclusion [G. Koyano, T. Okuhara, M. Misono, J. Am. Chem. Soc., 120 (1998) 767.] that the reversible oxidation and reduction between $(VO)_2P_2O_7$ and X_1 phase of $VOPO_4$ operates on the surface during the selective oxidation of *n*-butane with a relatively high selectivity for maleic anhydride, and showed that the surface X_1 phase formed by oxidation was reversibly reduced to the original $(VO)_2P_2O_7$ phase. However, β-$VOPO_4$ was once formed on the surface, the surface and the selectivity was not recovered by the reduction. It was confirmed by the IR investigation that the change of the surface were essentially reversible for the oxidation and reduction process between $(VO)_2P_2O_7$ and X_1 phase, but the oxidation to β-$VOPO_4$ changed irreversibly the surface. Furthermore, it was indicated that *n*-butane preferentially interacts with a Lewis acid site than a Brønsted acid site. © 2000 Elsevier Science B.V. All rights reserved.

Keywords: Vibrational spectroscopy; Surface redox process; Vanadyl pyrophosphate

1. Introduction

Vanadyl pyrophosphate ($(VO)_2P_2O_7$) is an active phase for selective catalytic oxidation of *n*-butane to maleic anhydride (abbreviated as MA) and is the main component of industrial catalysts for this process [1–3]. A Mars van Krevelen mechanism [4] is presumed to be involved in the selective oxidation to produce MA [5]. It has been claimed by some researchers that the redox cycle between V^{4+} and V^{5+} phase operate in this reaction [5–10]. On the other hand, Centi et al. proposed on the basis of a UV spectroscopic study [1,11] that redox between V^{3+} and V^{4+} is responsible for the selective oxidation. Recently, Gai et al. suggested based on TEM observation that V^{3+} species formed together with oxygen defects are responsible for the selective oxidation of *n*-butane [12,13].

As for the role of lattice oxygen, Pepera et al. [5] carried out an isotopic study using ^{18}O and concluded that the exchange between the sur-

* Corresponding author. Tel.: +81-3-5841-7271 ext. 7273; fax: +81-3-5841-7220; e-mail: gaku@appchem.t.u-tokyo.ac.jp

1381-1169/00/$ - see front matter © 2000 Elsevier Science B.V. All rights reserved.
PII: S1381-1169(99)00317-9

face layer of $(VO)_2P_2O_7$ and O_2 took place rapidly, but that between the surface and the solid bulk was very slow. We also showed that the diffusion of oxygen atom is limited to only a few surface layers during the reaction of *n*-butane with $^{18}O_2$ [8]. With respect to the active phase of this catalyst there have been quite a few studies (see references in Ref. [10]). Morishige et al. reported that the surface phosphorous rich phase is active for MA production [14]. Matsuura et al. [15] reported β and β″ phases, which have structures close to $(VO)_2P_2O_7$ are highly active. However, the true active sites are still controversial [1–3,5–16].

We have studied the redox process of the surface and bulk of the $(VO)_2P_2O_7$ and concluded that local redox cycles on the surface, very similar to the bulk redox between $(VO)_2P_2O_7$ and X_1 phase, are responsible for the selective formation of maleic anhydride, by using Raman spectroscopy, XPS, XRD, and EXAFS [10]. Here, the X_1 phase is the V^{5+} phase we reported previously [17], and contains V(=O)–O–V pair sites as those in $(VO)_2P_2O_7$. This phase shows XRD pattern and Raman spectrum similar to δ-$VOPO_4$ [18], and the same XRD pattern to β″ phase [15]. However, most of the measurements in our previous studies [9,10], i.e., Raman spectroscopy, XRD, XPS, and EXAFS, were carried out ex situ, so that the possible changes of the surface before or during the measurements could not be excluded. To solve the problem, in situ measurements have been attempted in the present study.

In situ Raman spectroscopy is the one of the powerful methods to study the VPO system [6,7,9,10,19]. Schrader's group examined the oxidation process of $(VO)_2P_2O_7$ to β-$VOPO_4$ with $^{18}O_2$ [19]. Abdelouahab et al. [6] concluded that V^{5+} phases, γ-$VOPO_4$, formed on the surface is active for the selective oxidation. We applied in situ Raman spectroscopy in the present study. Above mentioned methods of characterization, such as Raman spectroscopy and EXAFS, all provide the information of solid bulk, not limited to the surface. Since only surface few layers are involved in this reaction, as indicated by the tracer studies [5,8], the surface characterization is important for this catalytic system. Hence, we investigated in this study the surface by IR observation of CO adsorption at low temperature. Recently, the adsorption of CO has been used to measure the surface properties of various catalysts [20,21]. CO is a very weak base and its interaction with the surface sites is very moderate, especially at low temperature.

We report here the results obtained by using in situ Raman investigation of $(VO)_2P_2O_7$ and IR observation of low temperature adsorption of CO. The results indicate that the surface redox process between $(VO)_2P_2O_7$ and X_1 phase actually took place in a reversible way under the *flow* reaction conditions of the selective oxidation of *n*-butane when the butane/oxygen ratio in the feed was varied.

2. Experimental

2.1. Preparation of $(VO)_2P_2O_7$

Two kinds of precursor, vanadium hydrogen phosphate hemihydrate ($VOHPO_4 \cdot 0.5H_2O$), P-1 and P-3, were prepared as reported previously [22]. P-1 was prepared by the so-called aqueous solvent method and P-3 was obtained from the so-called organic solvent method. The solids showed the XRD pattern of $VOHPO_4 \cdot 0.5H_2O$ [23].

Vanadyl pyrophosphate ($(VO)_2P_2O_7$), C-1 and C-3, were obtained from P-1 and P-3, respectively, by the treatment at 823 K in an N_2 flow for 5 h. The C-1 and C-3 obtained were calcined in the stream of dry air (90 ml min^{-1}) at 733 K for 2 h (C-1) and 0.5 h (C-3). Then the catalysts were dispersed in water to form slurries, and the slurries were stirred for 3 h at room temperature. The catalysts were filtered and washed with water. The structures of C-1 and C-3 were confirmed by using XRD [22]. The BET surface areas of C-1 and C-3 were determined to be 10 and 78 $m^2\ g^{-1}$, respectively.

2.2. Preparation of $VOPO_4$

X_1 phase was synthesized from NH_4HVPO_6 as described previously [17]. An aqueous solution of $NH_4H_2PO_4$ ($NH_4H_2PO_4$; 0.8 mol, H_2O; 600 ml) containing V_2O_5 powder (0.04 mol) was boiled for 0.5 h and then cooled to room temperature to obtain precipitate, NH_4HVPO_6. The resulting solid was then treated in an O_2 flow at 823 K for 5 h to form X_1 phase. Bulk structure of X_1 phase ($VOPO_4$) was confirmed by XRD [17]. The BET surface area was 28 m^2 g^{-1}.

β-$VOPO_4$ was prepared by the calcination of $VOHPO_4 \cdot 0.5H_2O$ at 873 K in an O_2 flow for 10 h [17]. The surface area of β-$VOPO_4$ was about 3.2 m^2 g^{-1}. XRD pattern for β-$VOPO_4$ was consistent with the one reported previously [17].

2.3. In situ Raman spectroscopy

In order to observe the changes in the structure of the catalyst under steady-state reaction conditions, an in situ Raman cell was constructed as illustrated in Fig. 1 [24]. With this cell, the sample can be treated at 823 K under the reaction gases. The temperature was calibrated by measuring the melting points of zinc and tin. Raman spectra were recorded with a Laser Raman Spectrometer (Jasco, NR-1800) using the 514.5 nm Ar laser (NEC GLS3261J). The sample powders were placed on a glass sample holder and pre-treated under the same conditions as the steady state reaction (see below). The power of laser was usually set below 20 mW to avoid the damage of the samples.

2.4. IR study of low temperature CO / n-butane adsorption

The sample disk (self support, 20 mmϕ, ca. 20 mg) was set in an in situ cell and evacuated at 773 K for 1 h. Then, it was cooled to $\sim$90 K, and a predetermined amount of CO (6.82×10^{-6} mol) or *n*-butane (1.36×10^{-4} mol) was introduced. IR spectra were recorded at 90 K with a JASCO FT-IR 550 spectrometer. Oxidation treatment of the sample was carried out in the cell by introducing 200 Torr of O_2 at 733 K for 1 h. Reduction treatment was done in the presence of 10 Torr of *n*-butane at 733 K for 1 h. Both treatments were given to the sample after the adsorbed CO was completely eliminated by the evacuation at 733 K.

2.5. Characterization of catalysts

X-ray diffraction (XRD) patterns were obtained with an X-ray diffractometer (MAC Science MXP^3) using Cu Kα radiation ($\lambda = 1.5405$ Å). All the phases were confirmed by XRD.

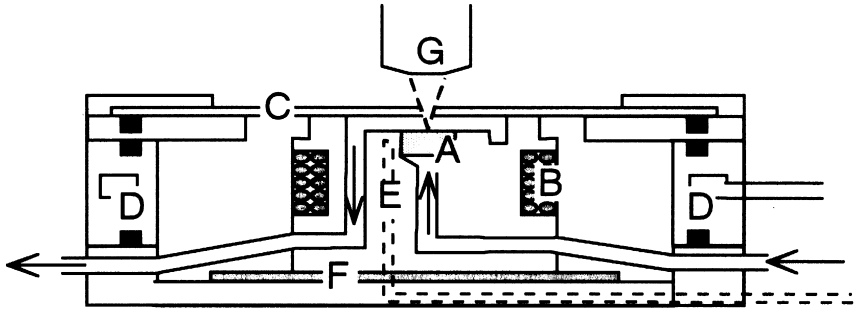

Fig. 1. Schematic illustration of in situ Raman cell. (A) Sample, (B) heater coil, (C) quartz window, (D) cooling water, (E) thermocouple, (F) heat insulator, and (G) objective lens. Arrows indicate the flow of reactant gas.

Surface areas of the catalysts were measured by BET method using N_2 adsorption with Micromeritics ASAP-2000, after the samples were treated in vacuum at 573 K for 1 h.

2.6. Catalytic oxidation of n-butane

Catalytic oxidation of *n*-butane was performed in a flow reactor at 733 K. Prior to the reaction, 70 mg of catalyst was treated in N_2 (60 cm^3 min^{-1}) at 773 K for 1 h. First, the reaction was performed with the gas composition of *n*-butane 1.5% (17%, O_2 content in parentheses). This is for the ordinary reaction conditions. Then the partial pressure of *n*-butane was decreased to 0.75% (18.5%), and to 0.25% (19.5%), all balanced with N_2. After this series of experiments, the catalyst was treated in a flow of air (20 cm^3 min^{-1}) for 2 h at the same temperature. Then, the partial pressure of *n*-butane was increased again to 0.25% (19.5%, O_2 content), 0.75% (18.5%), and 1.5% (17%), all balanced with N_2. Total flow rate of the gas mixture was varied to maintain the conversion level of *n*-butane to be $\sim$50% at each stage. In each stage of the reaction, the reaction was continued till a steady state was obtained. Products were analyzed by using two gas chromatographs; one (Shimadzu GC, GC-8, TCD) equipped with a silica gel column (4 mmϕ, 4.5 mm) for CO_2, and an MS-13X column (4 mmϕ, 1 m) for CO, O_2, and N_2 and the other (Yanaco GC, G-2800, FID) equipped with a Porapak QS column (4 mmϕ, 4.5 m) for MA and *n*-butane.

3. Results

3.1. Changes in Raman spectra under the oxidizing and reducing reaction conditions

The Raman spectra of C-3 changed as shown in Fig. 2, when the partial pressure of *n*-butane was decreased and subsequently increased. The selectivities of MA at each stage of partial pressure are summarized in Table 1. Parent C-3

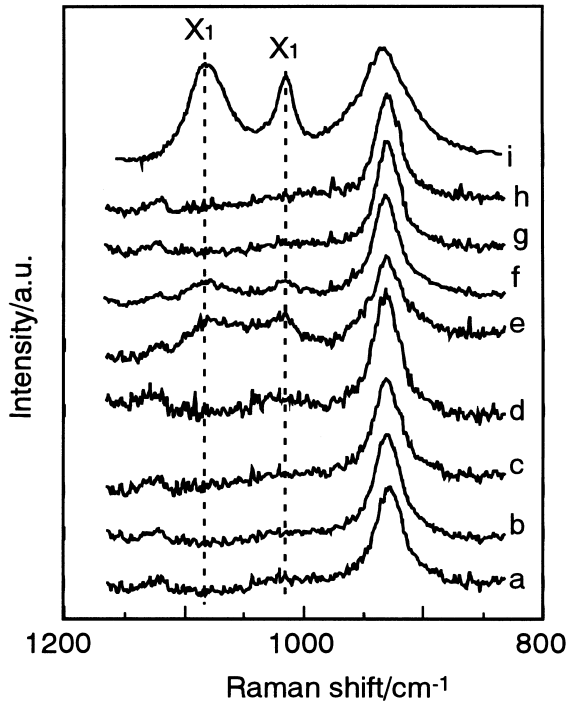

Fig. 2. Changes in Raman spectra of $(VO)_2P_2O_7$ (C-3) under steady state reaction. (a) the parent C-3. Partial pressure of *n*-butane was decreased from (b) 1.5% to (c) 0.75%, (d) 0.25%, and then (e) 0%. Then, it was increased from 0% to (f) 0.25%, (g) 0.75%, and then (h) 1.5%. All balanced with air. (i) X_1 phase. All spectra were recorded at 733 K. Flow rate: (b) and (h); 20 cm^3 min^{-1}, (c) and (g); 30 cm^3 min^{-1}, (d) and (f) 40 cm^3 min^{-1}, (e); 39 cm^3 min^{-1}.

showed a single peak at 930 cm^{-1} (Fig. 2, spectrum a), which is assigned to P–O–P stretching [25]. At room temperature, the P–O–P stretching mode appears at 923 cm^{-1}. With an increase in the temperature, the peak shifted to a higher frequency. This is probably because the angle of the P–O–P is variable depending on the temperature [25]. After 2 h of the steady state reaction, the spectrum showed the single peak due to $(VO)_2P_2O_7$ (Fig. 2b), and the MA selectivity was 52.4%. Upon the decrease of the *n*-butane content to 0.75%, there was little change observed either in the spectrum (Fig. 2c) or in the selectivity (48.8%). When the partial pressure of *n*-butane was set at 0.25%, the selectivity decreased to 23.4%, though the spectrum did not change much. Considering the fact

Table 1
Changes of the selectivity of maleic anhydride with the change of partial pressure of *n*-butane over $(VO)_2P_2O_7$ (C-3)

Partial pressure of C_4H_{10} (%)	Conversion (%)	Selectivity (%)	Raman spectrum	Phase[c]
1.5[a,d]	53.8	52.4	Fig. 2b	P
0.75[a,e]	52.0	48.8	Fig. 2c	P
0.25[a,f]	56.8	23.4	Fig. 2d	P (+X)
0.25[b,f]	56.0	22.8	Fig. 2f	P + X
0.75[b,e]	51.3	44.1	Fig. 2g	P
1.5[b,d]	45.5	61.7	Fig. 2h	P

[a] Partial pressure of butane (O_2 content) was decreased stepwise from 1.5 (17)% to 0.75 (18.5)% and then 0.25 (19.5)% after N_2 treatment of the catalyst at 773 K, balanced by N_2.
[b] Partial pressure of butane (O_2 content) was increased stepwise from 0.25 (19.5)% to 0.75 (18.5)% and 1.5 (17)% after treatment under air at 733 K, balanced by N_2.
[c] P: $(VO)_2P_2O_7$, X: X_1.
[d] Flow rate: 20 cm^3 min^{-1}.
[e] Flow rate: 30 cm^3 min^{-1}.
[f] Flow rate: 40 cm^3 min^{-1}.

that new peaks due to X_1 phase clearly appeared at 1016 and 1084 cm^{-1} by the subsequent oxidation by air (Fig. 2i), it is probable that a very weak band existed at 1016 cm^{-1} in spectrum d although the peak was not evident. Slight differences in the positions and the relative intensities between these peaks and those observed at 298 K by ex situ measurements [10] are merely due to the difference in the temperature of measurement. As the partial pressure of *n*-butane increased after the oxidation step (spectrum e), the peaks corresponding to X_1 phase decreased (Fig. 2f and g). When the peaks totally disappeared (spectrum h), the selectivity was recovered to 61.7%.

The results of the same procedure applied to C-1 are shown in Fig. 3. The selectivities of MA at each stage are summarized in Table 2. Parent C-1 showed a single peak at 930 cm^{-1} (Fig. 3, spectrum a). Under the reaction conditions, a new small peak corresponding to X_1 phase (1016 cm^{-1}) increased (spectra b–d). For the *n*-butane pressure of 1.5 and 0.75%, MA selectivities were still high (46.7 and 43.8%, respectively). When the partial pressure of *n*-butane was set at 0.25%, the selectivity decreased to 20.9%. After 2 h of air treatment, new three peaks in addition to the peaks due to X_1 phase were observed at 888, 988, and 1065 cm^{-1} (Fig. 3, e). Those three new peaks were coincident with the peaks of β-$VOPO_4$ (spectrum i, Fig. 3). As the partial pressure of *n*-butane increased after the oxidation by air, the peaks corresponding to X_1 phase and β-$VOPO_4$ decreased (Fig. 3g and h), and no peak other than $(VO)_2P_2O_7$ was observed (cf. Fig. 3, spectrum i). However, the selectivity at the steady state conditions still remained low (29.3%).

3.2. FT-IR observation of surface oxidation and reduction by using low temperature CO adsorption

Fig. 4 shows the IR spectra of CO adsorbed on VPO catalysts at about 90 K. All the spectra presented are those after the subtraction of the spectrum of VPO recorded before CO adsorption. Four peaks at 2141, 2170, 2179 and 2205 cm^{-1} were observed in the CO stretching vibration region (Fig. 4a). In the ν(OH) region, a reverse peak was observed at 3661 cm^{-1} and a new band appeared at 3462 cm^{-1}. As shown in spectrum b in Fig. 4, the evacuation at 90 K resulted in the decrease of the bands at 2141 and 2170 cm^{-1}. Simultaneously, the 3462 cm^{-1} band decreased and a very broad peak remained at a similar position. When the temperature was increased in vacuum (ca. 5 K min^{-1}), the band at 2179 cm^{-1} decreased gradually and disappeared before the temperature reached 190 K

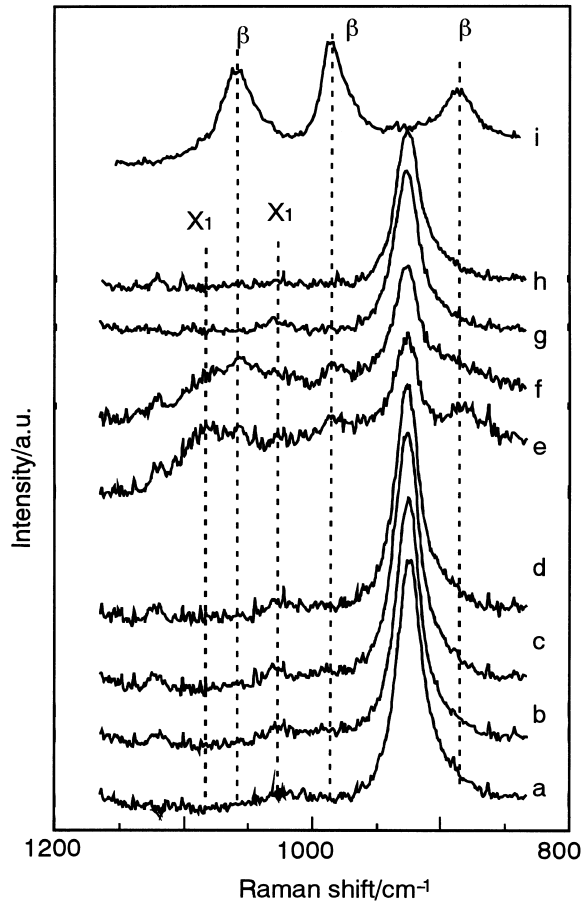

Fig. 3. Changes in Raman spectra of $(VO)_2P_2O_7$ (C-1) under steady state reaction. (a) shows the C-1. Partial pressure of *n*-butane was decreased from (b) 1.5% to (c) 0.75%, (d) 0.25%, and then (e) 0%. Then, it was increased from 0% to (f) 0.25%, (g) 0.75%, and then (h) 1.5%. All balanced with air. (i) β-$VOPO_4$. All spectra were recorded at 733 K. Flow rate: (b) and (h); 20 cm^3 min^{-1}, (c) and (g); 30 cm^3 min^{-1}, (d) and (f) 40 cm^3 min^{-1}, (e); 39 cm^3 min^{-1}.

(spectra c–e). The broad band at around 3460 cm^{-1} also disappeared. The band at 2205 cm^{-1} still remained even after the 190 K evacuation.

Effects of preoxidation and prereduction on IR spectra of CO adsorbed on $(VO)_2P_2O_7$ are shown in Fig. 5. As shown in spectrum a, four peaks in the CO stretching region, a reverse peak at 3661 cm^{-1} (decrease upon CO adsorption) and a peak at 3462 cm^{-1} in the OH vibration region were observed. When $(VO)_2P_2O_7$ was preoxidized at 733 K for 1 h by O_2, IR spectrum of CO subsequently adsorbed at 90 K was very different. The bands at 2205, 2179, and 3462 cm^{-1} disappeared (spectrum b), but a small and broad band at around 3462 cm^{-1} remained. It is remarkable that spectrum b was close to the IR spectrum of CO adsorbed on X_1 phase (spectrum d). Then the sample was evacuated at 733 K for 1 h and reduced by *n*-butane at 733 K for 1 h, and CO was introduced at 90 K. The recovery of the peaks at 2205 and 2179 cm^{-1} was noted (compare spectrum a and c). CO adsorbed on β-$VOPO_4$ shows two peaks at 2179 and 2170 cm^{-1} (spectrum e). When CO was introduced after the reduction of β-$VOPO_4$, the 2205 cm^{-1} band did not appear (spectrum f).

The effect of adsorption of *n*-butane was also examined by using CO adsorption at 90 K (Fig. 6), and the changes in the peak area are summa-

Table 2
Changes of the selectivity of maleic anhydride with the change of partial pressure of *n*-butane over $(VO)_2P_2O_7$ (C-1)

Partial pressure of C_4H_{10} (%)	Conversion (%)	Selectivity (%)	Raman spectrum	Phase[c]
1.5[a,d]	72.1	46.7	Fig. 3b	P
0.75[a,e]	68.7	43.8	Fig. 3c	P + X
0.25[a,f]	74.8	20.9	Fig. 3d	P + X + β
0.25[b,f]	71.7	15.8	Fig. 3f	P + X + β
0.75[b,e]	71.3	28.0	Fig. 3g	P
1.5[b,d]	71.3	29.3	Fig. 3h	P

[a] Partial pressure of butane (O_2 content) was decreased stepwise from 1.5 (17)% to 0.75 (18.5)% and then 0.25 (19.5)% after N_2 treatment of the catalyst at 773 K, balanced by N_2.
[b] Partial pressure of butane (O_2 content) was increased stepwise from 0.25 (19.5)% to 0.75 (18.5)% and 1.5 (17)% after treatment under air at 733 K, balanced by N_2.
[c] P: $(VO)_2P_2O_7$, X: X_1, β: β-$VOPO_4$.
[d] Flow rate: 20 cm^3 min^{-1}.
[e] Flow rate: 30 cm^3 min^{-1}.
[f] Flow rate: 40 cm^3 min^{-1}.

rized in Table 3. When *n*-butane was introduced on to $(VO)_2P_2O_7$ after evacuation at 733 K for 1 h, no change was observed in the OH stretching region (spectrum a) and several peaks due to CH vibration appeared in 2800–3000 cm^{-1}. Since butane molecules was significantly adsorbed on the wall of the cell, it was difficult to estimate the amount of *n*-butane adsorbed on the sample. Spectrum b shows the results of the

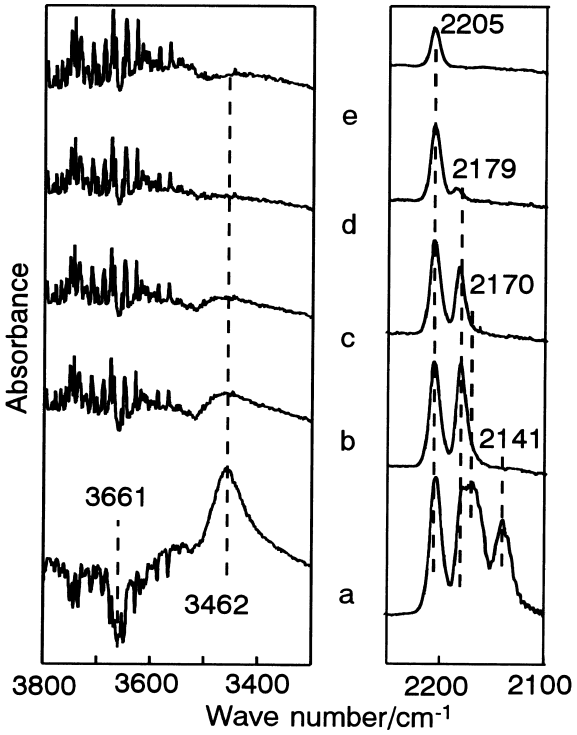

Fig. 4. IR spectra of CO adsorbed on $(VO)_2P_2O_7$ (C-3) at (a) 90 K. Then, (a) was evacuated at (b)90 K, (c) 150 K, (d) 170 K, and (e) 190 K.

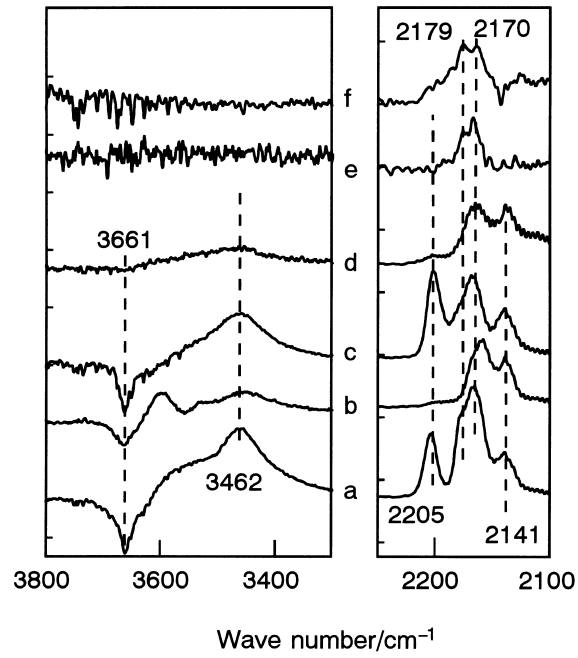

Fig. 5. IR spectra of CO adsorbed at 90 K on pretreated $(VO)_2P_2O_7$ (C-3). (a) C-3, (b) C-3 preoxidized at 773 K for 1 h. (c) (b) was evacuated at room temperature and reduced by *n*-butane at 733 K for 1 h. (d) X_1 phase, (e) β-$VOPO_4$, and (f) (e) was evacuated at room temperature reduced by *n*-butane at 733 K for 1 h.

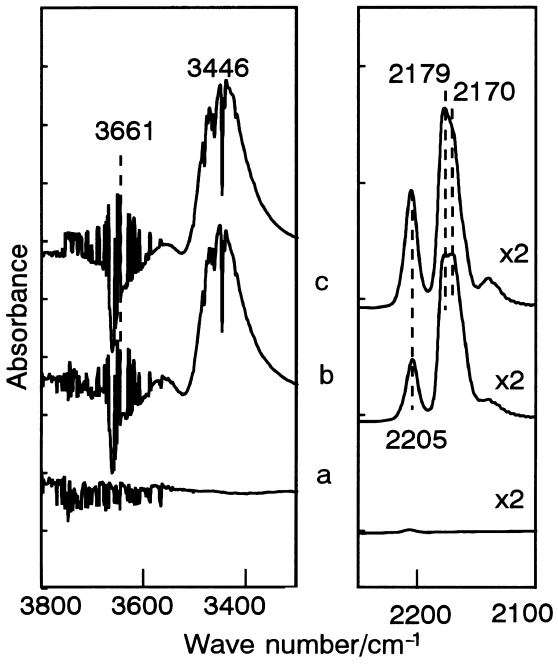

Fig. 6. IR spectra of (a) *n*-butane adsorbed on $(VO)_2P_2O_7$ (C-3) at 90 K. (b) CO was introduced after *n*-butane adsorption at 90 K. (c) IR spectra of CO adsorbed on C-3 at 90 K.

CO introduction after *n*-butane adsorption. The bands at the same wave numbers which were present in the absence of *n*-butane were observed, but the intensity of the peak at 2205 cm^{-1} was smaller.

4. Discussion

4.1. IR assignment of CO adsorbed and the surface structure

Recently, we reported that X_1 phase is responsible for selective MA formation, and proposed its structure by using electron diffraction, EXAFS, and Raman spectroscopy [9,10]. However, all these methods give the information of solid bulk and the actual surface structure cannot be directly evaluated. Even XPS contains the information of the bulk of more than 20 Å depth. In this study, we obtained additional information about the surface structure by using low temperature CO adsorption.

As shown in Fig. 4, four peaks in the CO stretching region (2205, 2179, 2170, and 2141 cm^{-1}) were observed upon CO adsorption on fresh $(VO)_2P_2O_7$ at 90 K. The peak at 3462 cm^{-1} peak can be assigned from its peak position [20,21] to acidic OH group interacting with CO, and the reverse peak at 3661 cm^{-1} to the original OH group of which the peak shifted to 3462 cm^{-1} upon CO adsorption. The 2141 cm^{-1} band is assigned to physisorbed CO in the case of zeolites and silica [20,21,26], so that the same assignment may be applied in the present case. Peaks at 2141, 2170, and 3462 cm^{-1} disappeared by evacuation at 90 K, and the reverse peak at 3661 cm^{-1} also disappeared simultaneously. Therefore, it is concluded that when CO adsorbs on the acidic OH group having IR peak at 3661 cm^{-1} its position shifts to 3462 cm^{-1} and the ν(CO) band appears at 2170 cm^{-1}. Further evacuation by increasing temperature decreased both the very broad peak at 3460 cm^{-1} and the peak at 2179 cm^{-1}, keeping the ratio nearly constant. Thus, the band at 3460 cm^{-1} may be assigned to another acidic OH group which shows the band of adsorbed CO at 2179 cm^{-1}. The results in the literature that the CO adsorbed on acidic proton of zeolites was observed in the region of 2156–2175 cm^{-1} [20,21,26] are consistent with the present assignments. It is expected that the position of the CO band absorbed on more acidic OH group

Table 3
Peak area of CO adsorbed on $(VO)_2P_2O_7$

	C_4H_{10} [a]	CO after C_4H_{10} [b]	CO[c]
2205 cm^{-1}	–	0.72	1.64
2177 + 2170 cm^{-1}	–	4.54	4.51

Temperature; 90 K. CO; 6.82×10^{-6} mol, *n*-butane; 1.36×10^{-4} mol.
Data are estimated from Fig. 6.
[a] Spectrum a.
[b] Spectrum b.
[c] Spectrum c.

appears at a higher shifts to a lower frequency so that the acid strength of OH observed at 2179 cm^{-1} is presumably stronger than OH at 2170 cm^{-1}.

As for the surface OH group, V–OH and P–OH are possibly present. Both V–OH and P–OH show OH stretching band at around 3660 cm^{-1} [27–29]. It is not possible to assign the above two bands unambiguously to either V–OH or P–OH, but it is to be remarked that Spielbauer et al. [27] reported that the CO adsorbed on P–OH shows the ν(CO) band at 2177 cm^{-1}.

Since only the peak at 2205 cm^{-1} was observed above 190 K without any peaks in the OH region, the band may correspond to CO adsorbed on Lewis acid sites [30]. If one considers that the oxidation state of V in fresh $(VO)_2P_2O_7$ observed by XPS was close to +4 [9,31], the band of CO on Lewis acid site (2205 cm^{-1}) may be $V^{4+} \cdots CO$, as in the case of V_2O_5/SiO_2 [30].

4.2. Redox cycle producing maleic anhydride

The surface redox mechanism on $(VO)_2P_2O_7$ is considered to proceed between V^{4+} and V^{5+} [8–10], and hence V^{5+} phases formed on the surface by the oxidation are thought to be important for the MA formation [5,8–10], while some researchers claim the importance of V^{3+} sites on the surface [1,11–13].

As shown in Fig. 2, X_1 phase was observed after the O_2 treatment. After the reaction in the presence of *n*-butane, the surface X_1 phase may exist (Fig. 2, spectrum b–d), but it was not clearly observed because the amount was small (less than 20% of the surface [10]). On the other hand, X_1 phase was observed in the case of C-1 under the reaction conditions in the presence of *n*-butane (Fig. 3, spectrum b–d). This is probably due to the difference in the amount of oxidized surface layers as indicated by our previous study [32]. When C-1 was treated under O_2 flow after the reaction, β-$VOPO_4$ increased. This is in agreement with the results that X_1 phase was formed first by the oxidation of C-1 under O_2 flow, then α and β-$VOPO_4$ [33]. X_1 phase may be transformed to β-$VOPO_4$. α-$VOPO_4$ was not detected in the present study, probably because the amount was small.

For C-3, after the X_1 phase formed by air treatment was reduced, the MA selectivity was recovered. However, once β-$VOPO_4$ was formed on the surface by decreasing *n*-butane pressure (Fig. 3e), MA selectivity was not fully recovered by the increase in the *n*-butane pressure even after β-$VOPO_4$ totally disappeared in Raman spectrum (Table 2). These results clearly demonstrate that the oxidation of $(VO)_2P_2O_7$ to X_1 phase by O_2 and the reduction of X_1 phase to $(VO)_2P_2O_7$ by *n*-butane take place reversibly under the reaction conditions, though the redox cycle between $(VO)_2P_2O_7$ and β-$VOPO_4$ is not reversible. The reason for the relatively low MA selectivity under the condition of 0.25% of *n*-butane partial pressure may be due to the consecutive oxidation of MA by the excess oxygen [10]. This is consistent with the fact that the MA selectivity was low in the reaction between surface X_1 phase and *n*-butane when the average oxidation state of the surface was high [10]. The irreversible change of the surface during the redox between $(VO)_2P_2O_7$ and β-$VOPO_4$ can be a cause of the deactivation.

Raman spectroscopy is a bulk technique so that the above mentioned observations may not exclude the possibility that there was a difference between the surface and bulk and the surface behaved differently. In this respect the low temperature adsorption of CO would provide useful information about the surface. After the oxidation at 733 K (Fig. 5, spectrum b), the state of surface became very close to that of X_1 phase (Fig. 5, spectrum d), and was distinctly different from that of β-$VOPO_4$. After the reduction of the oxidized $(VO)_2P_2O_7$ (Fig. 5, spectrum c), the surface recovered (compare spectrum c with spectrum a in Fig. 4). This clearly supports that the redox cycle between $(VO)_2P_2O_7$ and X_1 phase also proceeds reversibly on the surface. On the other hand, the reduction of β-$VOPO_4$ did not form any de-

tectable amount of Lewis acid site which was observed with $(VO)_2P_2O_7$ (Fig. 5, spectrum e). Therefore, it supports the conclusion that once β-$VOPO_4$ is formed on the surface of $(VO)_2P_2O_7$, the surface will not be recovered to that of $(VO)_2P_2O_7$.

4.3. Reaction on the surface

Selective oxidation of *n*-butane to MA is considered to proceed consecutively as follows: butane → butene → butadiene → furan → MA [1]. In the case of butane oxidation, $(VO)_2P_2O_7$ showed a high MA selectivity, but when butene and butadiene was used as the feed, the selectivity of $(VO)_2P_2O_7$ was comparable with or less than that of α- or β-$VOPO_4$ [34]. Thus, the activation of butane, dehydrogenation, is the important step to control the selectivity. Pepera et al. [5] concluded from the results of isotope effect by using deuterated butanes that dehydrogenation at methylene position is the rate-determining step. Busca et al. [35] reported based on the IR observation of adsorbed acetonitrile that V^{4+} site is a relatively strong Lewis acid site and presumed that the Lewis acid site subtracts methylene hydrogen of *n*-butane, Ai [36] together with Puttock and Rochester [37] also reported a correlation between acidity and reactivity.

Fig. 6 shows the effect of butane adsorption on $(VO)_2P_2O_7$ and Table 3 summarizes the change of the peak area accompanied. After the introduction of *n*-butane, no change was observed in the OH region, showing that butane did not interact with Brønsted acid site. Peak areas of the bands at 2179 and 2170 cm^{-1} of $(VO)_2P_2O_7$ with and without butane were almost the same. On the other hand, the peak area of the CO on the Lewis acid site was decreased after butane adsorption (spectrum b in Fig. 6). These results indicate that butane preferably interacts with Lewis acid site rather than with Brønsted acid site. Since Lewis acid site was not formed by the reduction of β-$VOPO_4$ (Fig. 5, spectrum f), which showed a low selectivity in *n*-butane oxidation, Lewis acid site (V^{4+}) must be important in controlling the selectivity.

5. Conclusion

We have demonstrated by using techniques for bulk and surface characterization that the reversible redox between $(VO)_2P_2O_7$ and X_1 phase produces MA selectively. Redox between $(VO)_2P_2O_7$ and β-$VOPO_4$ is not reversible and once β-$VOPO_4$ is formed, the surface and the MA selectivity irreversibly change. IR observation of CO adsorbed at low temperature indicated that *n*-butane preferably adsorbed at Lewis acid site (probably V^{4+}), and was activated there.

References

[1] G. Centi, F. Trifiro, J.R. Ebner, V.M. Franchetti, Chem. Rev. 88 (1988) 55.
[2] B.K. Hodnett, Catal. Rev. Sci. Eng. 27 (1985) 373.
[3] G. Centi, Catal. Today 16 (1993) 5.
[4] P. Mars, D.W. van Krevelen, Chem. Eng. Sci. 3 (1995) 41.
[5] M. Pepera, J.L. Callahan, M.J. Desmond, E.C. Milberger, P.R. Blum, N.J. Bremer, J. Am. Chem. Soc. 107 (1985) 4883.
[6] F.B. Abdelouahab, R. Olier, N. Guilhaume, F. Lefebvre, J.C. Volta, J. Catal. 134 (1992) 151.
[7] G.H. Hutchings, A.D. Chomel, R. Olier, J.C. Volta, Nature 368 (1994) 41.
[8] M. Misono, K. Miyamoto, K. Tsuji, T. Goto, N. Mizuno, T. Okuhara, in: G. Centi, F. Trifiro (Eds.), Stud. Surf. Sci. Catal., New Developments in Selective Oxidation, Elsevier, Amsterdam, 1990, p. 605.
[9] G. Koyano, T. Okuhara, M. Misono, Catal. Lett. 32 (1995) 205.
[10] G. Koyano, T. Okuhara, M. Misono, J. Am. Chem. Soc. 120 (1998) 767.
[11] F. Cavani, F. Trifiro, Chemtech 24 (1994) 18.
[12] P.L. Gai, K. Kourtakis, Science 267 (1995) 661.
[13] P.L. Gai, Acta Cryst. B 53 (1997) 346.
[14] H. Morishige, J. Tamaki, N. Miura, N. Yamazoe, Chem. Lett. (1990) 1513.
[15] I. Matsuura, A. Mori, M. Yamazaki, Chem. Lett. (1987) 1897.
[16] D. Ye, A. Satsuma, A. Hattori, T. Hattori, Y. Murakami, Catal. Today 16 (1993) 113.
[17] T. Shimoda, T. Okuhara, M. Misono, Bull. Chem. Soc. Jpn. 58 (1985) 2163.

[18] E. Bordes, P. Courtine, J. Chem. Soc. Chem. Commun., (1985) 294.
[19] T.P. Moser, G.L. Schrader, J. Catal. 128 (1991) 113.
[20] J.A. Lercher, C. Grundling, G. Eder-Mirth, Catal. Today 27 (1996) 353.
[21] H. Knözinger, in: R.W. Joyner, R.A. van Santen (Eds.), Elementary Reaction Steps in Heterogeneous Catalysis, Kluwer Academic Publisher, Netherlands, 1993, p. 267.
[22] H. Igarashi, K. Tsuji, T. Okuhara, M. Misono, J. Phys. Chem. 97 (1993) 7065.
[23] J.W. Johnson, D.C. Johnston, A.J. Jacobson, J.F. Brody, J. Am. Chem Soc. 106 (1984) 8123.
[24] T. Saito, G. Koyano, M. Misono, Chem. Lett. (1997) 415.
[25] T.P. Moser, G.L. Schrader, J. Catal. 104 (1987) 99.
[26] A. Zecchina, S. Bordiga, G. Spoto, D. Scarano, G. Petrini, G. Leofanti, M. Padovan, C.O. Areán, J. Chem. Soc. Faraday Trans. 88 (1992) 2959.
[27] D. Spielbauer, G.A.H. Mekhemer, T. Riemer, M.I. Zaki, H. Knözinger, J. Phys. Chem. B 101 (1997) 4681.
[28] H. Kamata, K. Takahashi, C.U.I. Odenbrand, Catal. Lett. 53 (1998) 65.
[29] G. Busuca, G. Centi, F. Trifiro, V. Lorenzelli, J. Phys. Chem. 90 (1986) 1337.
[30] A.A. Davydov, A.A. Budneva, N.G. Maksimov, React. Kinet. Catal. Lett. 20 (1982) 93.
[31] P. Delichère, K.E. Béré, M. Abon, Appl. Catal. A: General 172 (1998) 295.
[32] G. Koyano, F. Yamaguchi, T. Okuhara, M. Misono, Catal. Lett. 41 (1996) 149.
[33] G. Koyano, Thesis, The Univ. of Tokyo, 1997.
[34] K. Miyamoto, N. Mizuno, T. Nitadori, T. Okuhara, M. Misono, Chem. Lett. (1988) 303.
[35] G. Busca, G. Centi, F. Trifiro, V. Lorenzelli, J. Phys. Chem. 90 (1986) 1337.
[36] M. Ai, J. Catal. 100 (1986) 336.
[37] S.J. Puttock, C.H. Rochester, J. Chem. Soc., Faraday Trans. I 82 (1986) 2773.